Phosphate removal from water using an iron oxide impregnated strong base anion exchange resin

T. Nur, M.A.H. Johir, P. Loganathan, T. Nguyen, S. Vigneswaran*, J. Kandasamy

Faculty of Engineering and Information Technology, University of Technology, Sydney, Broadway, NSW 2007, Australia.

*corresponding author:

S. Vigneswaran

Phone**:** +61 2 9514 2641, Fax: +61 2 9514 2633

Mailing address: PO Box 123, Broadway NSW 2007, Australia

E-mail: s.vigneswaran@uts.edu.au

Abstract:

Removing phosphate from water is important as it causes eutrophication, which in turn has a harmful effect on aquatic life, resulting in a reduction in biodiversity. On the other hand, recovery of phosphate from phosphorus containing wastewater is essential for developing an alternative source of phosphorus to overcome the global challenge of phosphorus scarcity. Phosphate removal from aqueous solutions was studied using an iron oxide impregnated strong base anion exchange resin, Purolite FerrIX A33E in batch and fixed-bed column experiments. Phosphate adsorption in the batch study satisfactorily fitted to the Langmuir isotherm with a maximum adsorption capacity of 48 mg P/g. In the column study, increase in inlet phosphate concentration (5-30 mg P/L), and filtration velocity (2.5-10 m/h) resulted in faster breakthrough times and increase in breakthrough adsorption capacities. Increase in bed height (3-19 cm) also increased adsorption capacity but the breakthrough time was slower. The breakthrough data were reasonably well described using the empirical models of Bohart-

Adams, Thomas, and Yoon-Nelson, except for high bed heights. Phosphate adsorbed was effectively desorbed using 1M NaOH and the adsorbent was regenerated after each of three adsorption/desorption cycles by maintaining the adsorption capacity at > 90% of the original value. Greater than 99.5% of the desorbed P was recovered by precipitation using $CaCl_2$.

Keywords: anion exchange resin, fixed-bed column, breakthrough curve, phosphorus, phosphate, adsorption.

1. Introduction

Phosphorus (P) is an essential nutrient for the growth of plants and microorganisms. It is also an important chemical element for many industries and a major nutrient contaminant in water. It is released to water bodies in the form of organic and inorganic phosphates by domestic, mining, industrial and agricultural activities and municipal discharges. Excessive concentration of P in water causes eutrophication. Eutrophication is a major environmental problem as it can lead to abundant development of aquatic plants, including algae, threaten fish and other aquatic life, and disturb the ecological balance of organisms present in the water. The excessive P in water should be removed for controlling eutrophication and maintaining a sustainable green environment for future generations. To control eutrophication, environmental protection agencies in many countries have recommended that total P should not exceed 0.005-0.1 mg P/L in natural water bodies [1,2].

Several physical, biological and chemical processes have been investigated for the removal of dissolved phosphates in water and wastewaters. These processes include adsorption/ion exchange, chemical precipitation/coagulation, crystallization and membrane filtration / reverse osmosis. Of the various methods of P removal, adsorption/ion exchange methods are promising, because they are simple and economical, result in less sludge

production and therefore experience minimal disposal problems [3]. Furthermore, these methods seem to be the most suitable for small water supplies contaminated by P because of its simplicity, effectiveness, selective removal in the presence of other ions, easy recovery of P and relatively low cost [4]. These methods are also able to handle shock loadings and operate over a wide range of temperatures.

The performances of the adsorbents with reference to phosphate removal have been reported in literature with varying degrees of success [3]. Generally, ion exchangers are able to effectively remove nitrate from water, but they have not been successful in removing phosphate. For example, Gupta et al. [5] reported that Purolite 500A anion exchange resin had a Langmuir adsorption capacity of 64 mg N/g for nitrate adsorption whereas it had only 7 mg P/g for phosphate adsorption. Therefore, they used two columns in series, one with Purolite for removing nitrate followed by the other with hydrous ferric oxide for the removal of phosphate from water containing both these anions. Others used polymeric anion exchanger bound with ferric oxide nanoparticles to successfully remove phosphate [4,6]. These studies showed that adsorbents containing ferric oxide are required for effectively remove phosphate. Purolite FerrIX A33E media is another nanoparticle derived resin designed to selectively remove arsenic (arsenate and arsenite) from water supply [7]. This resin unites a unique blend of hydrous iron oxide nanoparticles that have a very high attraction for arsenic with a durable, non-friable, spherical polymer substrate. As this resin was found to be effective in removing arsenic anions, it is expected to have strong affinity for phosphate anions as well, because phosphate like arsenic is specifically adsorbed on iron oxides [3]. However, no detailed study has been conducted on phosphate adsorption by this ion exchange resin.

The aim of the present research is to study and model the removal of phosphate from synthetic wastewater employing the ion exchange resin, Purolite FerrIX A33E in batch and

fixed-bed column systems. The effects of bed height, initial phosphate concentration and filtration velocity were investigated in the column study. The empirical models of Bohart-Adams, Thomas and Yoon-Nelson were tested for their ability to describe the column adsorption data. A study was also conducted to develop a suitable method to regenerate the adsorbent for reuse, as well as recovery of the desorbed P for beneficial use.

2. Material and methods

2.1. Ion exchange resin

A commercially available and reasonably economical iron oxide impregnated Type II hybrid strong base anion exchange resin, Purolite FerrIX A33E obtained from the Purolite Company, U.S.A. [7] was used as the adsorbent in this study. This adsorbent is a blend of hydrous iron oxide nanoparticles and highly porous polystyrene cross-linked with divinylbenzene polymer having an arsenic operating capacity of 0.5-4 g As/L and available in the form of spherical beads (0.3-1.2 mm diameter). The highly porous nature of the resin bead allows for maximum utilisation of the impregnated iron oxide. The polymer component of the adsorbent had positively charged quarternary ammonium functional groups with chloride as counter ion [8]. The resin contained 13% Fe.

2.2. Feed solutions

The feed solutions were prepared using KH_2PO_4 with distilled water spiked with different concentrations of phosphate (5-30 mg P/L). The pH of the solutions ranged from 7.2 to 7.6.

2.3. Chemical analysis

The analysis of phosphate ion was carried out using a Metrohm ion chromatograph (model 790 Personal IC) equipped with an auto sampler and conductivity cell detector. The separation was achieved using an A SUPP column 3 (150 mm x 4 mm). Na_2CO_3 (3.2

mmol/L) and $NaHCO_3$ (1.0 mmol/L) were used as mobile phase with a flow rate of 0.9 mL/min.

2.4. Batch adsorption experiment

Equilibrium adsorption experiments were conducted in a set of glass flasks with 100 mL solutions spiked with phosphate (10 mg P/L) and ion exchange resin concentrations of 0.1-10 g/L at room temperature (24 ± 1^{o}C). The suspensions were agitated in a flat shaker at a shaking speed of 120 rpm for 72 h to ensure that the adsorption equilibrium is reached. However, preliminary experiments showed that the adsorption equilibrium was achieved within 48 h. The experiments were duplicated and the average values were taken for data analysis. The difference between duplicate values was within ± 2%. The amount of phosphate adsorption at equilibrium, q_e (mg P/g), was calculated using equation (1),

$$q_e = \frac{(C_0 - C_e)V}{M} \quad (1)$$

where, C_0 = initial concentration of phosphate (mg P/L); C_e = equilibrium concentration of the phosphate (mg P/L); V = volume of the solution (L) and M = mass of adsorbent (g).

2.5. Column mode experiments

The fixed-bed column was made of 2.0 cm inner diameter pyrex glass tube. At the bottom of the column, a stainless steel sieve was attached followed by a layer of glass beeds in order to provide a uniform flow of the solution through the column. A known quantity (12-86 g) of the resin was packed in the column to yield the desired bed height (3-19 cm) of the adsorbent. Phosphate solutions of known concentrations (5, 10, 15, 20 and 30 mg P/L) was pumped upward through the column at a desired filtration velocity (2.5, 5.0 and 10.0 m/h) controlled by a peristaltic pump. The effluents at the outlet of the column were collected at

regular time intervals and the phosphate concentration was measured using ion-chromatograph.

The breakthrough curves show the loading behaviour of phosphate to be removed from solution in a fixed-bed column and are usually expressed in terms of adsorbed phosphate-P concentration (C_{ad}), inlet phosphate-P concentration (C_o), outlet phosphate-P concentration (C) or normalized concentration defined as the ratio of outlet phosphate concentration to inlet phosphate concentration (C/C_o) as a function of time. The maximum column capacity, q_{total} (mg P), for a given feed concentration and filtration velocity is equal to the area under the plot of the adsorbed phosphate-P concentration, C_{ad} ($C_{ad} = C_o - C$) (mg/L) versus effluent time (t, min) and is calculated from equation (2).

$$q_{total} = \frac{Q}{1000}\int_{t=0}^{t=total} C_{ad}\,dt \qquad (2)$$

Equilibrium uptake q_{eq} (mg P/g) or maximum capacity of the column is defined by equation (3) as the total amount of adsorbed phosphate-P concentration (q_{total}) per g of adsorbent (M) at the end of the total flow time:

$$q_{eq} = \frac{q_{total}}{M} \qquad (3)$$

The detention times of Purolite FerrIX A33E during fluidization are calculated using equation (4).

$$t = H/v \qquad (4)$$

where, t is the detention time (h), H is the column bed height (m) and v is the upflow filtration velocity (m/h).

2.6. Batch adsorption isotherm modelling

Batch adsorption data were modelled using Langmuir adsorption isotherm equation [9] expressed as follows:

$$Q_e = \frac{q_{max} K_L C_e}{1 + K_L C_e} \quad (5)$$

where, q_{max}= the maximum amount of the phosphate-P concentration per unit weight of the adsorbent (mg P/g), K_L = Langmuir adsorption constant (L/mg).

This model can be linearised as follows:

$$C_e/Q_e = 1/q_{max}\ K_L\ + C_e/q_{max} \quad (6)$$

2.7. Fixed bed column modelling

2.7.1. The Bohart-Adams model

The Bohart-Adams model [10] established the fundamental equations describing the relationship between C_t/C_o and t in a continuous flow system. The model expression is shown below:

$$\ln C_t/C_o = k_{AB} C_o t - k_{AB} N_o\ Z/F \quad (7)$$

where, C_o and C_t (mg P/L) are the inlet and effluent phosphate concentration, k_{AB} (L/mg.min) is the kinetic constant, F (cm/min) is the linear velocity calculated by dividing the filtration velocity by the column section area, Z (cm) is the bed depth of column and N_o (mg

P/L) is the saturation concentration. The values for k_{AB} and N_o were determined from the intercept and slope of the linear plot of $\ln(C_t/C_o)$ against time (t). The Bohart-Adams adsorption model was applied to experimental data to describe the initial part of the breakthrough curve.

2.7.2. The Thomas model

The Thomas model [11] assumes plug flow behaviour in the bed, and uses the Langmuir isotherm for equilibrium and second order reversible reaction for kinetics. This model is suitable for adsorption processes where the external and internal diffusion limitations are absent. The linearized form of the Thomas model can be expressed as follows:

$$\ln (C_o/C_t - 1) = k_{Th}q_oM/Q - k_{Th}C_ot \qquad (8)$$

where, k_{Th} (mL/min.mg) is the Thomas rate constant; q_o (mg P/g) is the equilibrium phosphate uptake per g of the Purolite resin; C_o (mg/L) is the inlet phosphate concentration; C_t (mg P/L) is the outlet phosphate concentration at time t; M (g) is the mass of adsorbent, Q (mL/min) is the filtration velocity and t (min) stands for filtration time. A linear plot of $\ln[(C_o/C_t)-1]$ against time (t) was employed to determine values of k_{Th} and q_o from the intercept and slope of the plot.

2.7.3. The Yoon–Nelson model

Yoon and Nelson [12] developed a model based on the assumption that the rate of decrease in the probability of adsorption of adsorbate molecule is proportional to the probability of the adsorbate adsorption and the adsorbate breakthrough on the adsorbent. The linearized form of the Yoon–Nelson model for a single component system is expressed as:

$$\ln [C_t/(C_o - C_t)] = k_{YN}t - \tau k_{YN} \quad (9)$$

where, k_{YN} (1/min) is the rate velocity constant, τ (min) is the time required for 50% phosphate breakthrough. A linear plot of $\ln [C_t/(C_o - C_t)]$ against sampling time (t) was used to determine values of k_{YN} and τ from the intercept and slope of the plot.

2.8. Regeneration of adsorbent and phosphate recovery

When the adsorbent Purolite FerrIX A33E was saturated with phosphate ions in the column, it was important to regenerate the adsorbent for the recovery of phosphate ions as well as the reuse of the adsorbent for further adsorption of phosphate. In this study, the column regeneration studies were carried out using different desorbing agents such as 1 M NaCl, 1 M Na_2SO_4, 1 M NaOH, and MQ water. The regeneration was performed by leaching the resin containing the adsorbed phosphate with the leaching solution at a filtration velocity 10 m/h for 30 min. Since phosphate was enriched through the adsorption process, the enriched phosphate was desorbed by the regeneration solutions and recovered as calcium phosphate by adding different concentrations of $CaCl_2$ to the leachate.

3. Results and discussion

3.1. Batch adsorption experiment

The results of the batch equilibrium adsorption experiment indicated that the removal efficiency of phosphate improved with increased resin dose due to increased availability of surface area for adsorption (Figure 1a). Approximately 90% removal of phosphate was achieved with a resin dose 1 g/L and the removal efficiency reached 97% with resin doses $\geq$ 5 g/L. The adsorption isotherm data (Figure 1b) satisfactorily fitted to the Langmuir adsorption model (data not shown) and the value of the maximum adsorption capacity was 48 mg P/g.

This adsorption capacity is among the highest values reported for most adsorbents in the literature (Table 1). The high adsorption capacity is probably due to the presence of nano-sized iron oxide particles in the adsorbent which can have adsorption capacity in the order of 145 mg P/g Fe [28]. Based on this adsorption capacity the contribution of the iron oxide to the total adsorption capacity of the Purolite resin is estimated to be 19 mg P/g resin (13% Fe in resin x 145 mg P/g). This amount of phosphate is adsorbed specifically by inner sphere surface complexation on iron oxide [3,13,14] and the remaining amount of phosphate is adsorbed by coulombic forces (outer-sphere complexation) on the quaternary ammonium functional group positive charges in the polymer component of the Purolite.

Figure 1

Table 1

3.2. Fixed-bed column studies

Adsorption of phosphate by Purolite FerrIX A33E is presented in the form of breakthrough curves (Figures 2-4). The breakthrough curves became less sharp when the mass transfer rates were decreased [29]. Since mass transfer rates were finite, the breakthroughs were diffused and exhibited an S-shape pattern.

Figures 2, 3, 4

3.2.1. Effect of adsorbent bed height

Figure 2 shows the breakthrough curves obtained for phosphate adsorption on the Purolite resin at bed heights of 3, 6, 12, 14, 16, 17 and 19 cm (12, 28, 56, 66, 76, 80 and 86 g of resin), at a constant filtration velocity 2.5 m/h and inlet concentration 20 mg P/L. Based on Figure 2 it is evident that at low bed heights, the breakthrough occurred faster than that at

high bed heights. This pattern of breakthrough at different bed heights is similar to the findings in other column studies reported on different adsorbents and adsorbates [30,31]. The starting time of saturation occurred after 3, 9, 13, 19, 23, 25 and 28 h when the bed height was 3, 6, 12, 14, 16, 17 and 19 cm, respectively, and 50% saturation was achieved within the interval of 5, 13, 21, 25, 31, 34 and 39 h, respectively. As the bed height increased, phosphate had more time to contact with the Purolite ion exchange resin as shown by the higher detention time (Table 2), resulting in more efficient removal of phosphate. Thus, the higher bed height resulted in a greater decrease in phosphate concentration in the effluent. The slope of the breakthrough curve decreased with increase in bed height as a result of broadened influent movement zone [31]. However, it is found that the complete pattern of adsorption breakthrough curve was formed at all bed heights. The adsorption of phosphate increased when bed height rose from 3 to 19 cm, because of the increased amount of adsorption sites available at higher bed heights.

3.2.2. Effect of initial phosphate concentration

The effect of increase in the influent phosphate concentration from 5 to 30 mg P/L on breakthrough curves is shown in Figure 3. The starting time of saturation occurred at 30, 23, 17, 15 and 13 h and 50% saturation was achieved after an operation period of 45, 28, 21, 19 and 15 h for the influent concentrations of 5, 10, 15, 20 and 30 mg P/L, respectively. The breakthrough time occurred faster and the breakthrough curves were sharper with increasing influent phosphate concentration. These results are consistent with nitrate adsorption on an ion exchange resin [32]. These results demonstrate that the change of concentration gradient affects the saturation rate and breakthrough time, or in other words, the diffusion process is concentration dependent. As the influent concentration increases, phosphate loading rate increases, so does the driving force for mass transfer, and decreases in the adsorption zone

length [33]. The extended breakthrough curve at low influent concentration indicates that a higher volume of solution can be treated.

3.2.3. Effect of filtration velocity

The effect of filtration velocity on the adsorption of phosphate on Purolite resin was investigated by varying the filtration velocity (2.5, 5.0 and 10.0 m/h) at a constant adsorbent bed height of 12 cm and the inlet concentration of 30 mg P/L. The breakthrough generally occurred faster and the breakthrough curve was steeper with higher filtration velocity (Figure 4). The time to reach the plateau of C_t/C_0 increased significantly with a decrease in the filtration velocity. The plateau of C_t/C_0 occurred at 9, 15, and 23 h for the inlet filtration velocity of 10, 5.0, and 2.5 m/h with the values of C_t/C_0 of 0.90, 0.85, and 0.83, respectively. Faster breakthrough of adsorbates and steeper breakthrough at higher filtration velocities have also been reported elsewhere for adsorption onto other adsorbents [31,34].

At a lower filtration velocity, phosphate had more time to contact with Purolite resin as indicated by the higher detention time (Table 4), which allowed the diffusion of the phosphate ions into the pores of the adsorbent, resulting in a higher proportion of the removal of the influent phosphate ions in the column (lower C_t/C_o). However, the quantity of phosphate ions removed was lower at lower filtration rate (Table 4), due to the lower amounts of phosphate ions (lower bed volumes) passing through the column per unit time. Mixed results have been reported in the literature on the effect of filtration velocity on adsorption capacity. Increase of filtration velocity was found to decrease the adsorption of Cu on activated carbon [31], whereas increase of filtration velocity increased adsorption of Pb on oil palm fibre [35]. However, Hekmatzadeh et al. [32] reported that filtration velocity had no effect on the adsorption of nitrate on an ion exchange resin. The differences in the effects of filtration velocity may be due to the type of adsorbent and adsorbate, and experimental

conditions such as filtration velocities, bed heights and influent concentrations used in the different studies.

3.3. Empirical modelling

3.3.1. Bohart-Adams model

The model's fit to the experimental data was good for all the inlet phosphate concentrations ($R^2 \geq 0.72$, Table 3) and filtration velocities ($R^2 \geq 0.80$, Table 4), but only for the low bed heights (3-14 cm, $R^2 \geq 0.80$, Table 2). The values of k_{AB} calculated from the model decreased when inlet phosphate-P concentration and bed height increased, but it increased when the filtration velocity increased. The value of N_o increased with the increasing inlet concentration and bed height but decreased with increasing filtration velocity. The increase in k_{AB} with filtration velocity shows that the overall system kinetics was dominated by external mass transfer in the initial part of adsorption in the column [36].

3.3.2. Thomas model

The high R^2 values (0.80-0.98) obtained for the model fit to experimental data indicate that Thomas model described the column data very well (Tables 2, 3, 4). The model prediction of the column adsorption capacity (q_o) increased with bed height (Table 2), inlet phosphate concentration (Table 3), and filtration velocity (Table 4) consistence with the observations made earlier based on the breakthrough curves. The values obtained for q_o from the model are approximately equal to those calculated from the breakthrough curves.

3.3.3. Yoon–Nelson model

The experimental data fitted satisfactorily to Yoon-Nelson model for all phosphate concentrations and filtration velocities (R^2 = 0.76-0.99, Table 3 and 4) but, similar to Bohart-Adams model, the fit was good only at low bed heights (3-14 cm, $R^2 \geq 0.83$, Table 2). The

rate constant k_{YN} increased and the 50% breakthrough time (τ) decreased when both filtration velocity and inlet concentration increased (Tables 3 and 4), but the opposite trend occurred with increasing bed height (Table 2). With the increase of bed height, τ rose while k_{YN} fell, which was also observed for Cu adsorption on rice husk-based activated carbon [31].

Considering the values of R^2 for the models fits to the data and breakthrough curves, it can be concluded that all three models can be used to reasonably describe the behaviour of the adsorption of phosphate on the Purolite resin in a fixed-bed column. The exception is perhaps the use of the Bohart-Adams and Yoon-Nelson models at high bed heights, where the models' fits to the data were poor.

Table 2, 3, 4

3.4. Regeneration of Purolite resin

The phosphate adsorption capacity of the column was estimated by Thomas model to be 16.4 mg P/g, and by breakthrough curve calculation to be 12.9 mg/g (Table 4). Among the reagents used for the regeneration of Purolite resin, NaOH was found to be effective in desorbing the phosphate from the column. No detectable phosphate was desorbed using 1 M NaCl, Na_2SO_4 and water. The inability of the high concentrations of Cl^- and SO_4^{2-} in the Na salts in desorbing the phosphate ions from the adsorbent suggests that phosphate ions were strongly adsorbed specifically by inner sphere complexation probably on the Fe oxide component of the adsorbent [3, 13, 14]. This is consistent with the adsorption capacity of the iron oxide in the Purolite resin estimated in section 3.1 (19 mg P/g), which is more than the amount of phosphate adsorbed in the column, suggesting that all the phosphate in the column may have adsorbed to the iron oxide component of the resin. Only 60-70% of the adsorbed phosphate was desorbed by 0.5 M NaOH whereas 90-95% of the phosphate was desorbed by 1.0 M NaOH in 42 bed volumes. Approximately 70% phosphate was desorbed within 10 min

(14 bed volumes). The regenerated adsorbent was tested for reuse after every adsorption-desorption cycle using fresh 1M NaOH for each desorption cycle (Figure 5). The results showed that the efficiency of phosphate adsorption-desorption was nearly the same for two cycles and dropped a little in the third cycle. The decline in efficiency of adsorption/desorption was not more than 10%, indicating that the Purolite resin has good potential to adsorb phosphate and is reusable for at least three times. Further studies need to be conducted for higher number of adsorption/desorption cycles to determine the number of such cycles that can be performed without significantly reducing the adsorption capacity.

Figure 5

3.5. Recovery of desorbed phosphate

The effect of different concentrations of $CaCl_2$ added to the solution containing the desorbed phosphate on the reduction in solution concentration of phosphate is shown in Figure 6. The results showed that increase in $CaCl_2$ concentration decreased solution phosphate concentration, indicating that phosphate has been precipitated probably as calcium phosphate. Kuzawa et al. [17] showed that addition of $CaCl_2$ to desorbed phosphate solution can form calcium phosphate and hydroxyapatite compounds which have good fertiliser value. Midorikawa et al. [37] also proposed a P removal and recovery system with recycling of the alkaline desorbing solution similar to the method reported by Kuzawa et al. [17]. Recently this system was successfully tested in pilot plants in Japan and the United States [37,38]. If P removed from the water is economically recovered, it can partly overcome the perceived future scarcity of P when natural phosphate rock reserves will be exhausted [3].

Figure 6

4. Conclusions

Batch and fixed-column experimental results showed that Purolite FerrIX A33E is a potential adsorbent for removing phosphate from aqueous solutions. The batch adsorption was satisfactorily explained using the Langmuir isotherm while the column adsorption data fitted reasonably well to the empirical models of Bohart-Adams, Thomas and Yoon-Nelson. The Langmuir adsorption capacity was 48 mg P/g, whereas the column breakthrough adsorption capacity increased with increasing bed height, inlet phosphate concentration and filtration velocity; the highest adsorption capacity was found to be 16 mg P/g at the inlet concentration of 30 mg P/L, 12 cm bed height and 10 m/h filtration velocity. The adsorption capacity predicted by the Thomas model was also highest (23 mg P/g) for these experimental conditions. The Purolite resin could be regenerated by leaching the adsorbed phosphate with 1 M NaOH solution and reused for at least three times without significantly reducing the adsorption capacity. Finally, phosphate could be recovered from the exhausted desorption solution as calcium phosphate by adding $CaCl_2$.

Acknowledgements

This work was funded by Australian Research Council Discovery Research Grand (DP 1092603). We thank Vitachem for supplying the Purolite resin.

References

[1] ANZECC, National Water Quality Management Strategy: An Introduction to the Australian and New Zealand Guidelines for Fresh and Marine Water Quality. Australian Government Department of Sustainability, Environment, Water, Population and Communities, Canberra, Australia, 2000.

[2] D.K. Mueller, D.R. Helsel, Nutrients in the Nation's Waters--Too Much of a Good Thing? U.S. Geological Survey Circular 1136, 1996.

[3] P. Loganathan, S. Vigneswaran, J. Kandasamy, N.S. Bolan, Crit. Rev. Environ. Sci. Technol. (2013) (in press).

[4] L.M. Blaney, S. Cinar, A.K. Sengupta, Water Res. 41 (2007) 603-1613.

[5] M.D. Gupta, P. Loganathan, S. Vigneswaran, Sep. Sci. Technol. 47 (2012) 1785-1792.

[6] B.D. Martin, S.A. Parsons, B. Jefferson, Water Sci. Tech. 60 (2009) 2637-2645.

[7] www.purolite.com-Purolite FerrIX A33E , Technical data, ISO 9002.

[8] www.aquascotland.com/_product_33602/Ion_Exchange_Ferr.

[9] B.H. Hameed, I.A.W. Tan, A.L. Ahmad, Chem. Eng. J. 144 (2008) 235–244.

[10] G.S. Bohart, E.Q. Adams, J. Chem. Soc. 42 (1920) 523–529.

[11] H.C. Thomas, J. Am. Chem. Soc. 66 (1944) 1466–1664.

[12] Y.H. Yoon, J.H. Nelson, Am. Ind. Hyg. Assoc. J. 45 (1984) 509–516.

[13] E.A. Deliyanni, E.N. Peleka, N.K. Lazaridis, Sep. Purif. Technol. 52 (2007) 478-486.

[14] A. Genz, A. Kornmüller, M. Jekel, Water Res. 38 (2004) 3523-3530.

[15] J. Wang, Y. Zhang, C. Feng, J. Li, G. Li, J. Water Resour. Protect. 4 (2009) 260-264.

[16] F. Long, J. Gong, G. Zeng, L. Chen, X. Wang, J. Deng, Q. Niu, H. Zhang, X. Zhang, Chem. Eng. J. 171 (2011) 448-455.

[17] K. Kuzawa, Y. Jung, Y. Kiso, T. Yamada, M. Nagai, T. Lee, Chemosphere 62 (2006) 45-52.

[18] J. Ma, J.H. Lenhart, K. Tracy, J. Irrig. Drain. Eng. ASCE 137 (2011) 244-250.

[19] R. Mahmudov, C.P. Huang, Sep. Purif. Technol. 77 (2011) 294-300.

[20] W.E. Marshall, L.H. Wartelle, J. Chem. Technol. Biotechnol. 79 (2004) 1286-1292.

[21] D.J. Akhurst, G.B. Jones, M. Clark, D. McConchie, Environ. Chem. 3 (2006) 65-74.

[22] K. Sakadevan, H.J. Bavor, Water Res. 32 (1998) 393-399.

[23] J. Pradhan, J. Das, S. Das, R.S. Thakur, J. Colloid Interface Sci. 204 (1998) 169-172.

[24] Y. Li, C. Liu, Z. Luan, X. Peng, C. Zhu, Z. Chen, Z. Zhang, J. Fan, Z. Jia, J. Hazard. Mater. 137 (2006) 374-383.

[25] G. Gong, S. Ye, Y. Tian, Q. Wang, J. Ni, Y. Chen, J. Hazard. Mater. 166 (2009) 714-719.

[26] Y. Xue, H. Hou, S. Zhu, J. Hazard. Mater. 162 (2009) 973-980.

[27] L. Zeng, X. Li, J. Liu, Water Res. 38 (2004) 1318-1326.

[28] A. Zach-Maor, R. Semiat, H. Shemer, J. Colloidal Interface Sci. 357 (2011) 440-446.

[29] J.N. Cloutier, A. Leduy, R.S. Ramalho, Can. J. Chem. Eng. 63 (1985) 250-257.

[30] R.T. Ahmad, T.V. Nguyen, W.G. Shim, S. Vigneswaran, H. Moon, J. Kandasamy, Sep. Purif. Technol. 98 (2012) 46-54.

[31] N.K.E.M. Yahaya, I. Abustan, M.F.P.M. Latiff, O.S. Bello, M.A. Ahmad, J. Eng. Technol. 11 (2011) 248-252.

[32] A.A. Hekmatzadeh, A. Karimi - Jashani, N. Talebbeydokhti, B. Klove, Desalination 284 (2012) 22-31.

[33] J. Goel, K. Kadirvelu, C. Rajagopal, V.K. Garg, J. Hazard. Mater. 125 (2005) 211-220.

[34] V.C. Srivastava, B. Prasad, I.M. Mishra, I.D. Mail, M.M. Swamy, Ind. Eng. Chem. Res. 47 (2008) 1603-1613.

[35] J.T. Nwabanne, P.K. Igbokwe, Inter. J. Appl. Sci. Technol. 2 (2012) 106-115.

[36] Z. Aksu, F. Gonen, Process Biochem. 39 (2004) 599– 613.

[37] I. Midorikawa, H. Aoki, A. Omori, T. Shimizu, Y. Kawaguchi, K. Katsusai, T. Murakami, Water Sci. Tech. 58 (2008) 1601-1607.

[38] J. Fitzpatrick, H. Aoki, S. Koh, C. deBarbadillo, I. Midorikawa, M. Miyazaki, A. Omori, T. Shimizu, Proceed. Water Environ. Federation/IWA Nutrient Recovery Manage. Conf. (2011) 778-789.

Table 1. Comparison of Langmuir adsorption capacity for phosphate on Purolite FerrIX A33E with that on various other adsorbents in synthetic solutions

Adsorbent	**Experimental conditions (E, equilibrium concentration (mg P/L); I, initial concentration (mg P/L))**	**Adsorption capacity (mg P/g)**	**Reference**
Akagenite	25^{o}C, pH 7, E 1-250	60	[13]
Akagenite granulated	20^{o}C, pH 5.5, E 0-4	17-23	[14]
Activated alumina	20^{o}C, pH 5.5, E 0-4	12-14	[14]
Activated alumina	E 0-2	3.3	[15]
Iron/zirconium binary oxide	25^{o}C, pH 4, E 0-80	13.7	[16]
MgAlLDH (granular)	25^{o}C, pH 6.9, E 0-150	47.3	[17]
Zeolite	20^{o}C, E 0-40	0.13	[18]
Activated carbon	E 0-28	3.2	[19]
Activated carbon (granular)	20^{o}C, E 0-25	1.2	[18]
Anion exchange resin from soybean hulls	25^{o}C, pH 7, 10 g resin, I 0-620	20	[20]
Bauxsol	pH 5.2-6.2, E 0-43	14-15	[21]
Blast furnace slag	25^{o}C, E 0-600	44.2	[22]
Activated red mud	30^{o}C, pH 5.2, E 0-62	22.5	[23]
Activated red mud	25^{o}C, E 0-800	54, 113	[24]
Raw red mud	25^{o}C, E 0-800	38	[24]
Blast furnace slag	30^{o}C, E 0-11	29	[25]
Basic oxygen furnace slag	20^{o}C, E 0-120	11-20	[26]
Fly ash	E 0-900	20-26	[24]
Iron oxide tailings	20-21^{o}C, pH 6.6-6.8, E 0-130	5-8	[27]
Purolite A500P anion exchange resin	Resin dose 0.5-10 g/L, I 15	7	[6]
Purolite FerrIXA33E anion exchange resin	24^{o}C, pH 7.2-7.6, resin dose 0.1-10 g/L, I 10	48	This study

Table 2. The parameters of three models for different bed heights (initial concentration = 20 mg P/L and filtration velocity = 2.5 m/h)

Bed Height	**Bohart-Adams Model**			**Thomas Model**			**Yoon-Nelson Model**			**Breakthrough adsorption capacity**	**Detention time**
(cm)	k_{AB} (L/mg. min) x 10^{-5}	N_o (mg/L) x10^3	R^2	k_{Th} (mL/min.mg) x 10^{-2}	q_o (mg/g)	R^2	k_{YN} (1/min) x 10^{-3}	τ (min) x10^3	R^2	q_{eq} (mg/g)	t (h)
3	50.3	11.8	0.88	65.8	11.4	0.98	15.3	0.3	0.96	11.4	0.012
6	17.8	16.5	0.86	22.8	12.6	0.96	5.3	0.9	0.90	13.5	0.024
12	8.6	17.0	0.91	13.2	12.7	0.94	3.5	1.5	0.93	11.1	0.048
14	7.0	20.7	0.80	12.0	13.4	0.91	3.2	1.8	0.83	11.7	0.056
16	5.6	21.8	0.63	10.9	13.6	0.86	1.6	3.1	0.63	12.2	0.064
17	5.0	23.2	0.72	9.6	13.7	0.90	1.6	3.2	0.75	12.0	0.068
19	4.4	25.0	0.42	8.7	14.5	0.84	1.5	3.4	0.61	12.5	0.076

Table 3. The parameters of three models for different initial concentrations (bed height = 12 cm and filtration velocity = 2.5 m/h)

Influent concentration	**Bohart-Adams Model**			**Thomas Model**			**Yoon-Nelson Model**			**Breakthrough adsorption capacity**	**Detention time**
(mg P/L)	k_{AB}(L/mg. min) x 10^{-5}	N_o(mg/L) x10^3	R^2	k_{Th} (mL/min.mg) x 10^{-2}	q_o (mg/g)	R^2	k_{YN} (1/min) x 10^{-3}	τ (min) x10^3	R^2	q_{eq} (mg/g)	t (h)
5	14.1	8.4	0.83	24.8	4.7	0.88	0.9	3.3	0.81	4.1	0.048
10	13.5	11.1	0.72	19.8	7.4	0.89	2.1	2.2	0.76	6.9	0.048
15	11.7	12.8	0.93	18.6	7.6	0.89	2.8	1.5	0.76	7.0	0.048
20	11.2	15.3	0.84	17.7	11.3	0.91	3.3	1.4	0.82	11.4	0.048
30	9.2	20.0	0.90	16.1	12.8	0.94	4.1	1.3	0.85	13.2	0.048

Table 4. The parameters of three models for different filtration velocities (bed height = 12 cm and initial concentration = 30 mg P/L)

Filtration velocity	**Bohart-Adams Model**			**Thomas Model**			**Yoon-Nelson Model**			**Breakthrough adsorption capacity**	**Detention time**
(m/h)	k_{AB}(L/mg. min) x 10^{-5}	N_o (mg/L) x 10^3	R^2	k_{Th} (mL/min.mg) x 10^{-2}	q_o (mg/g)	R^2	k_{YN} (1/min) x 10^{-3}	τ (min) x 10^3	R^2	q_{eq} (mg/g)	t (h)
2.5	5.8	29.7	0.80	11.5	16.4	0.91	4.0	1.3	0.85	12.9	0.048
5.0	19.1	17.7	0.92	13.6	19.2	0.84	9.0	0.6	0.97	15.9	0.024
10.0	33.2	16.4	0.98	13.9	22.7	0.80	14.0	0.3	0.99	16.3	0.012

Figure captions

Figure 1. (a) Effect of Purolite FerrIX A33E resin dose on the efficiency of P removal from a solution containing PO_4-P concentration of 10 mg/L and (b) Langmuir Isotherm model fit for phosphate removal by the resin.

Figure 2. Breakthrough curves for different bed heights (initial phosphate concentration = 20 mg P/L and filtration velocity = 2.5 m/h)

Figure 3. Breakthrough curves for different inlet concentrations (bed height = 12 cm and filtration velocity = 2.5 m/h)

Figure 4. Breakthrough curves for different filtration velocities (bed height =12 cm and initial phosphate concentration = 30 mg P/L)

Figure 5. Breakthrough curves for phosphate desorption by 1 M NaOH in the column adsorption experiment (bed height 12 cm, initial concentration 30 mg P/L, filtration velocity 2.5 m/h) for three adsorption-desorption cycles of Purolite FerrIX A33E.

Figure 6. Supernatant concentrations of phosphate after $CaCl_2$ addition to the solution obtained by 1M NaOH leaching of Purolite resin after phosphate adsorption.

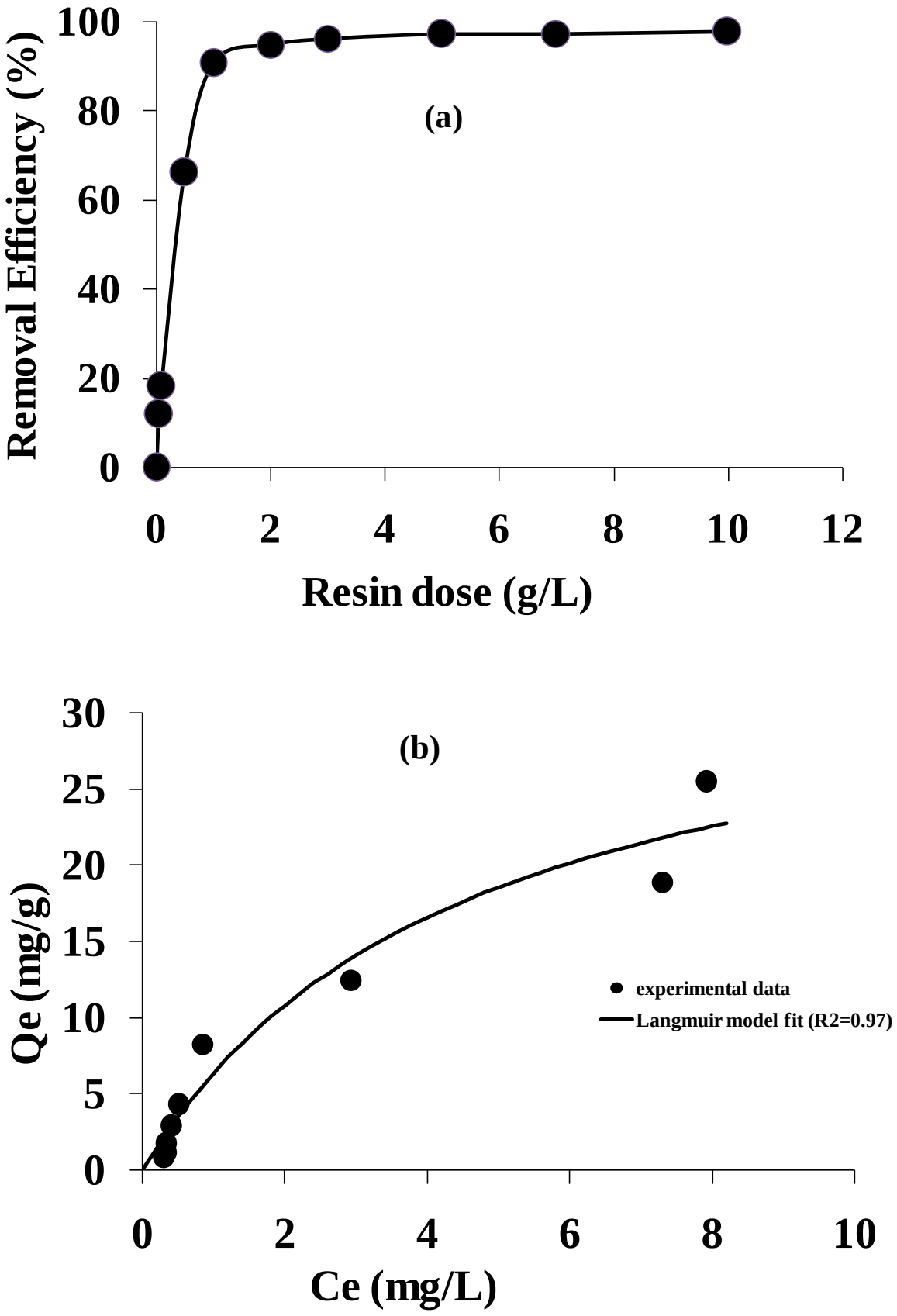
Removal Efficiency (%)
100
80
60
40
20
0
(a)
0
2
4
6
8
10
12
Resin dose (g/L)
Qe (mg/g)
30
25
20
15
10
5
0
(b)
experimental data
Langmuir model fit (R2=0.97)
0
2
4
6
8
10
Ce (mg/L)

Fig. 1

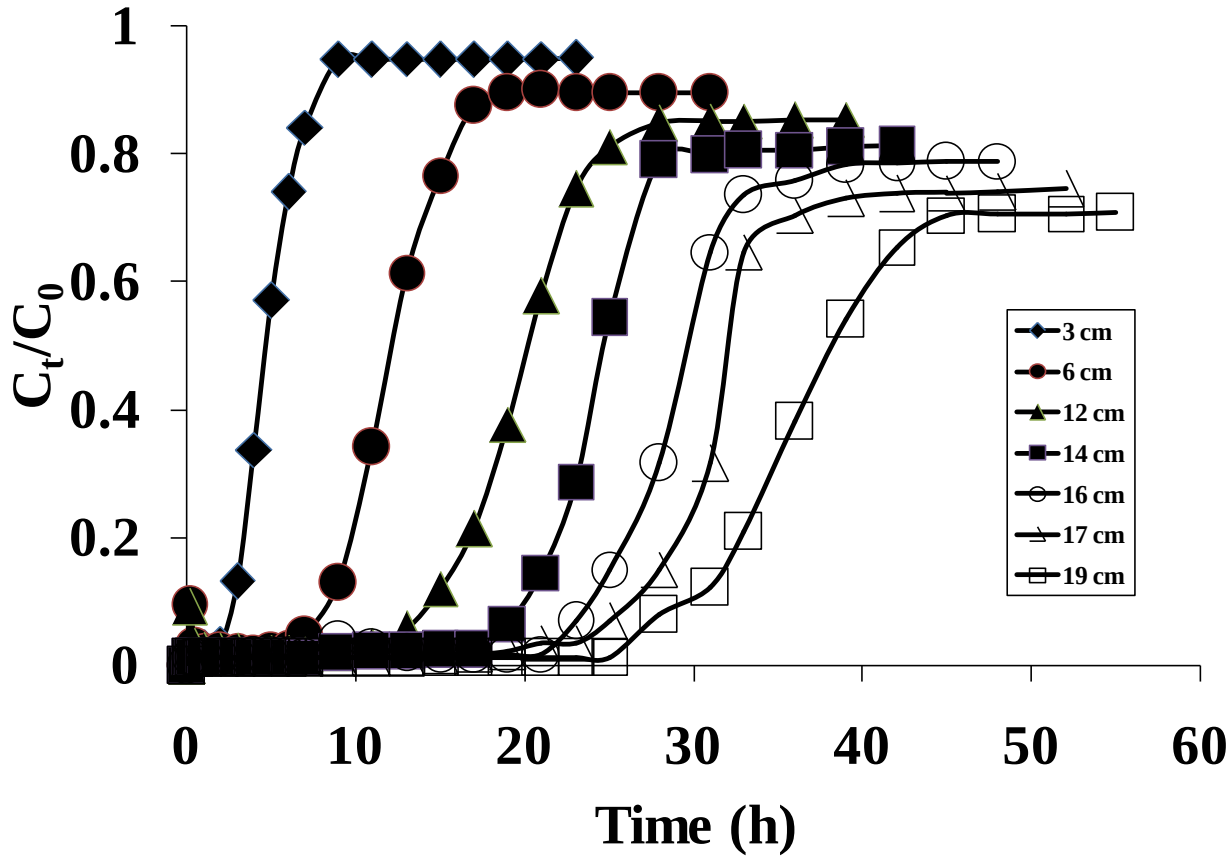
1
0.8
0.6
0.4
0.2
0
C_t/C_0
0
10
20
30
40
50
60
Time (h)
3 cm
6 cm
12 cm
14 cm
16 cm
17 cm
19 cm

Fig. 2

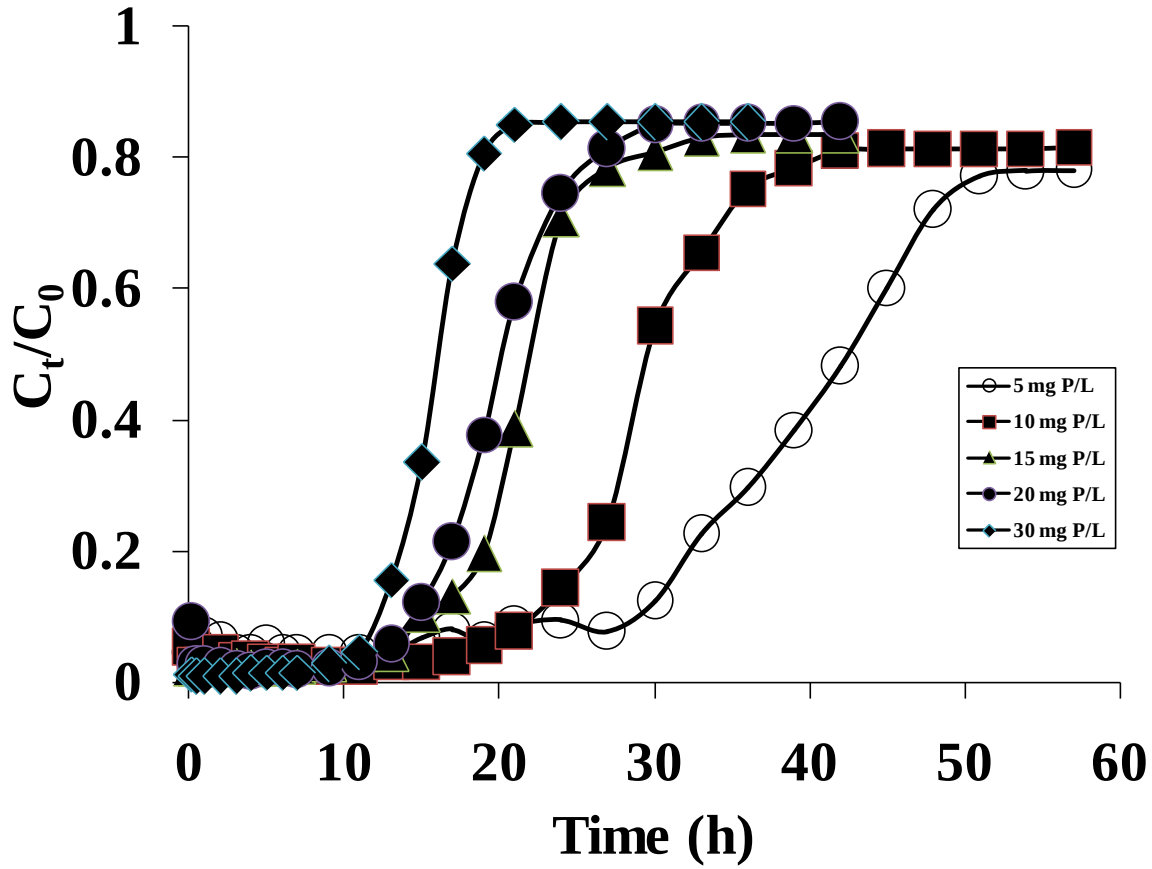
1
0.8
0.6
0.4
0.2
0
C_t/C_0
0
10
20
30
40
50
60
Time (h)
5 mg P/L
10 mg P/L
15 mg P/L
20 mg P/L
30 mg P/L

Fig. 3

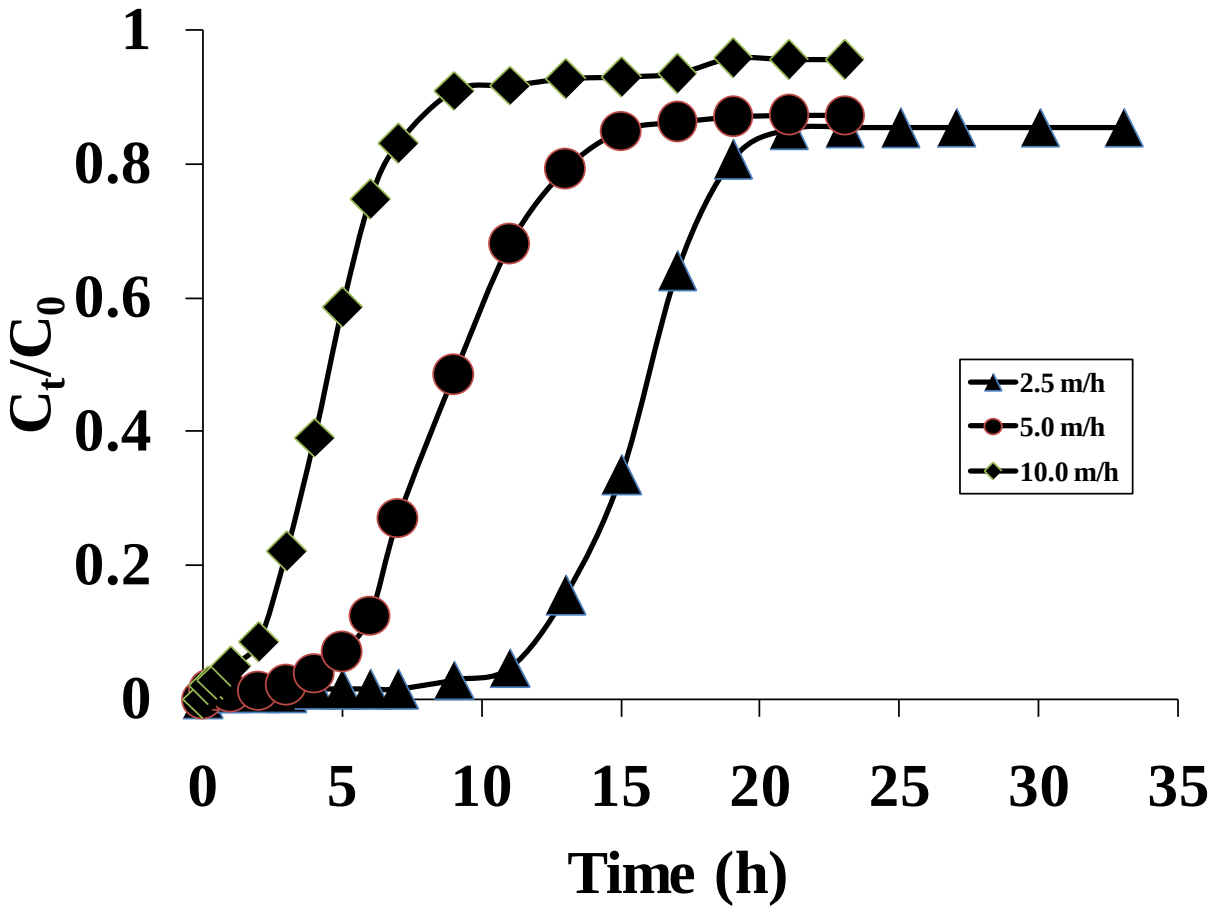

Fig. 4

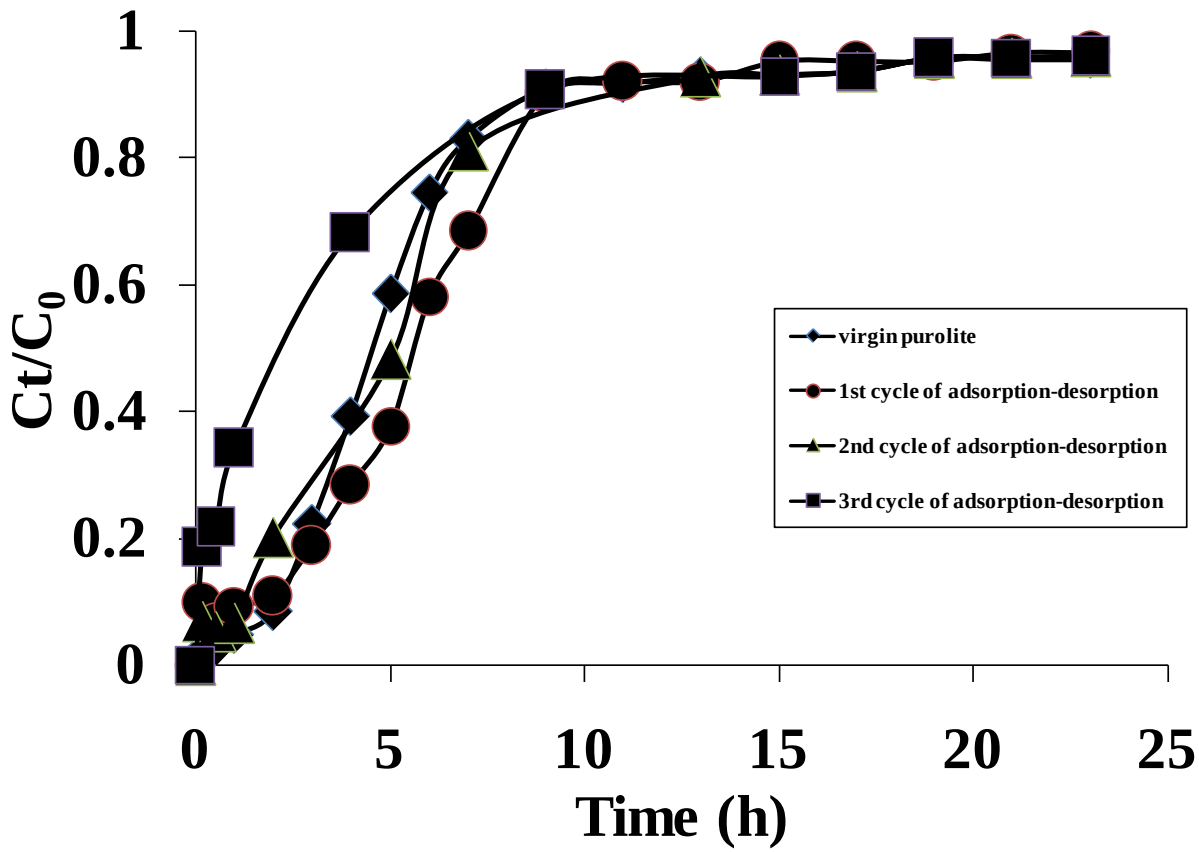
1
0.8
0.6
0.4
0.2
0
Ct/C0
0
5
10
15
20
25
Time (h)
virgin purolite
1st cycle of adsorption-desorption
2nd cycle of adsorption-desorption
3rd cycle of adsorption-desorption

Fig. 5

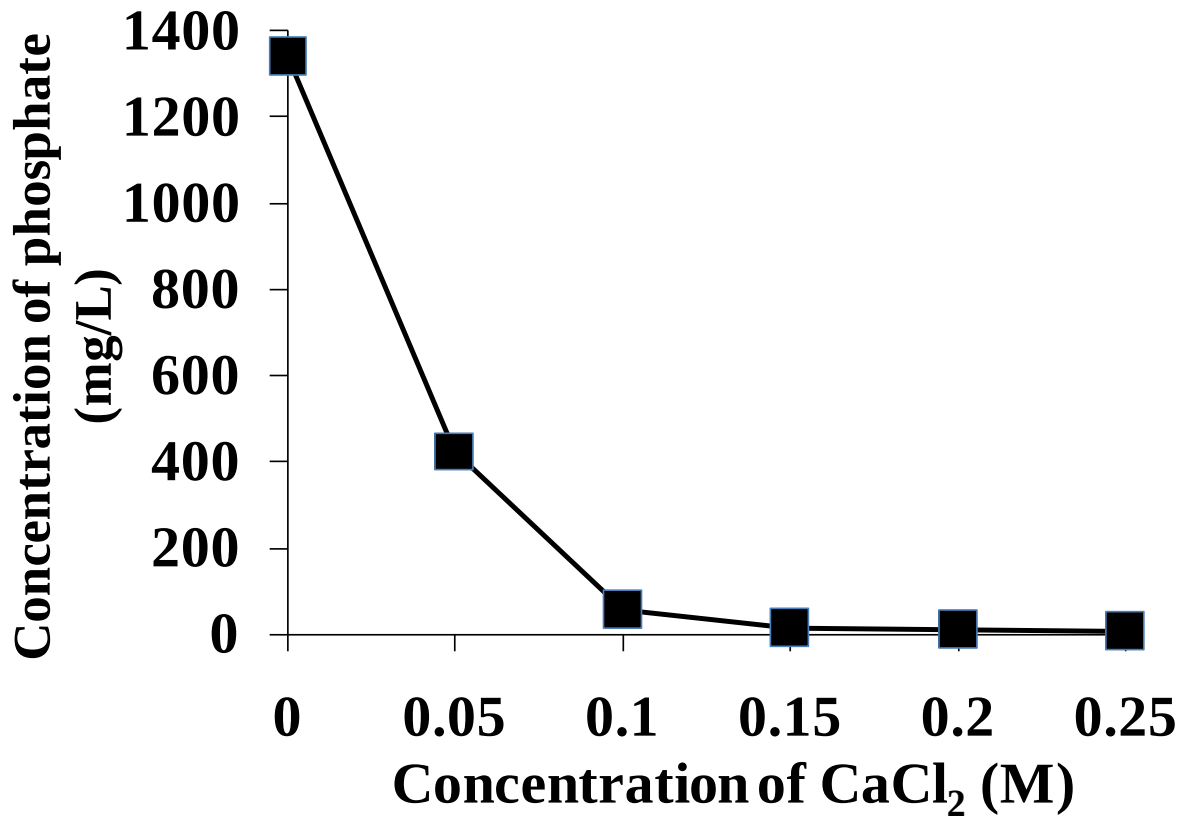
Concentration of phosphate (mg/L)
1400
1200
1000
800
600
400
200
0
0
0.05
0.1
0.15
0.2
0.25
Concentration of CaCl2 (M)

Fig. 6